CrossMark

Graphene-mediated band gap engineering of WO$_3$ nanoparticle and a relook at Tauc equation for band gap evaluation

Kaushik Baishya[1] · Joydwip S. Ray[1] · Pankaj Dutta[2] · Partha P. Das[3] · Shyamal K. Das[1]

Abstract
Engineering the band gap of semiconductors is often crucial in the quest for developing new and advanced technologies. In this report, the implication of graphene on the band gap optimization of tungsten trioxide (WO$_3$) is discussed. Simple one-step sol–gel process was followed to anchor WO$_3$ nanoparticles in graphene. Graphene induces a redshift in the band gap of WO$_3$. Band gap narrowing of 6.60% is observed for 7 wt% graphene-tethered WO$_3$. Interestingly, a profound difference is observed in estimating the band gap energy values following the usual Tauc equation. Our observation suggests that the differential form of Tauc equation is better suited to determine the band gap energy of inorganic semiconductors than the typical extrapolation method.

1 Introduction

The crowning of Nobel prize in Physics in 2010 for the discovery of two-dimensional graphene has set off unparalleled research activity globally to understand its fundamental properties, and consequently its technological aspects [1–11]. Establishing itself as a wonder material of the decade in the vast domain of materials science, graphene has unprecedentedly demonstrated its might in a plethora of applications. In the last few years, extensive research has been done to find viable pathways to use graphene in nanoelectronics, nanophotonics, energy storage devices, solar cells, biosensors, etc. [4–11]. This overwhelming success has been sustained due to the unique richness in the thermal, mechanical, optical and electrical properties of graphene [12–20].

The unique exuberant properties of graphene are simultaneously harnessed by developing graphene-based nanocomposites [21]. Researchers have demonstrated that the addition of an infinitesimal fraction of graphene in nanocomposites can substantially change the physicochemical properties of the conjugated components of the nanocomposites. For example, the glass transition temperature of polymethyl methacrylate is increased by 30 °C by the addition of 0.5 wt% functionalized graphene and the elastic modulus is increased by 80% with the addition of 1 wt% graphene [22]. The Al–graphene nanocomposite with 0.3 wt% graphene showed 62% enhancement in tensile strength compared to that of pristine Al [23]. The lithium and sodium battery performance of titanium dioxide is dramatically improved by the addition of 0.5 wt % and 2.28 wt% graphene, respectively [24, 25]. Graphene nanochannel-supported GaN LED shows 33% enhancement in the light output power with 25% and 30% reduction in junction temperature and thermal resistance, respectively [26]. Conversely, the conjugated components in graphene nanocomposites can also complement the properties of graphene. For instance, the core–shell quantum dot structure of ZnO and graphene induces an electronic band gap of 250 meV in graphene [27].

Therefore, in the present work, we systematically address the influence of graphene in tuning the band gap and optical

---

Kaushik Baishya and Joydwip S. Ray have contributed equally to this study.

Electronic supplementary material The online version of this article (doi:https://doi.org/10.1007/s00339-018-2097-0) contains supplementary material, which is available to authorized users.

✉ Partha P. Das
skdas@tezu.ernet.in

✉ Shyamal K. Das
daspm@nitk.ac.in

[1] Department of Physics, Tezpur University, Assam 784028, India

[2] Department of Physics, Dibrugarh University, Assam 786004, India

[3] Department of Physics, National Institute of Technology Karnataka, Surathkal 575,025, India

emission of tungsten trioxide (WO_3). WO_3 is chosen as the model material considering its immense technological importance. It is paramount to applications such as photovoltaics, photocatalysis, electrochromics and energy storage [28–31]. Furthermore, band gap engineering is often crucial to wring out additional benefits from traditional semiconductors. For instance, titanium dioxide starts to demonstrate visible light photoactivity if the band gap is engineered via nitrogen doping, which otherwise is UV light active [32]. Similarly, the band engineering (indirect to direct) of bulk silicon makes it plausibly an important light emitting active material [33, 34].

In this study, we observed that the energy band gap of WO_3 undergoes redshift in the presence of graphene. Moreover, a profound difference is observed in estimating the energy band gap values following the usual Tauc equation. We have found that the differential form of Tauc equation is better suited than the typical extrapolation method to estimate the band gap energy of semiconductors.

2 Experimental

2.1 Synthesis of graphene–WO_3 nanocomposite

Sodium tungstate was used as the tungsten precursor. Graphene (graphene platelet nanopowder) was obtained from Sisco Research Laboratories Pvt. Ltd. India. The graphene nanopowder was treated with concentrated HNO_3 for 24 h and washed thoroughly with distilled water several times. For the synthesis of WO_3–graphene composite, a certain amount (e.g., 10, 20, 30, 40, 50 mg) of acid-treated graphene was dispersed in 50 ml water by ultrasonication for 30 min.

Then, 1 g Na_2WO_4 was dissolved in the above solution. Following this, 8 ml of 3 N HCl was added to the solution under stirring condition. This resulted in a gray precipitate after 10 min. The precipitate was recovered by centrifugation and washed with deionized water and dried at 120 °C for 24 h. The dried product was further heated at 350 °C for 3 h in air at a heating rate of 5 °C min^{-1}. Pristine WO_3 was synthesized in a similar way except for the addition of graphene. The graphene–WO_3 composite is designated as G–WO_3 hereafter.

The crystallographic phase identification of the products was performed using powder X-ray diffraction (XRD; Rigaku; Cu-K$_\alpha$ radiation, $\lambda = 1.5418$ Å). The morphology was observed by scanning electron microscopy (SEM, JEOL JSM 6390LV) and transmission electron microscopy (TEM, FEI Technai T20; accelerating voltage 200 kV). Ultraviolet–visible (UV–Vis) spectroscopy was utilized for determining the optical absorption of the composites. The UV–Vis absorption spectra were recorded using Shimadzu UV 2450 spectrometer. The spectra were recorded using solid state measurement. All experiments were performed at room temperature (25 °C). Estimation of graphene content was done using thermogravimetric analysis (TGA, Mettler Toledo). TGA experiments were performed by heating the sample in air at a heating rate of 5 °C min^{-1}.

3 Results and discussion

The XRD patterns of pristine WO_3 and G–WO_3 are shown in Fig. 1a. The XRD patterns of both pristine WO_3 and G–WO_3 could be indexed to the hexagonal crystal structure of WO_3 (JCPDS 75-2187) with lattice parameters $a = b = 7.2980$ Å,

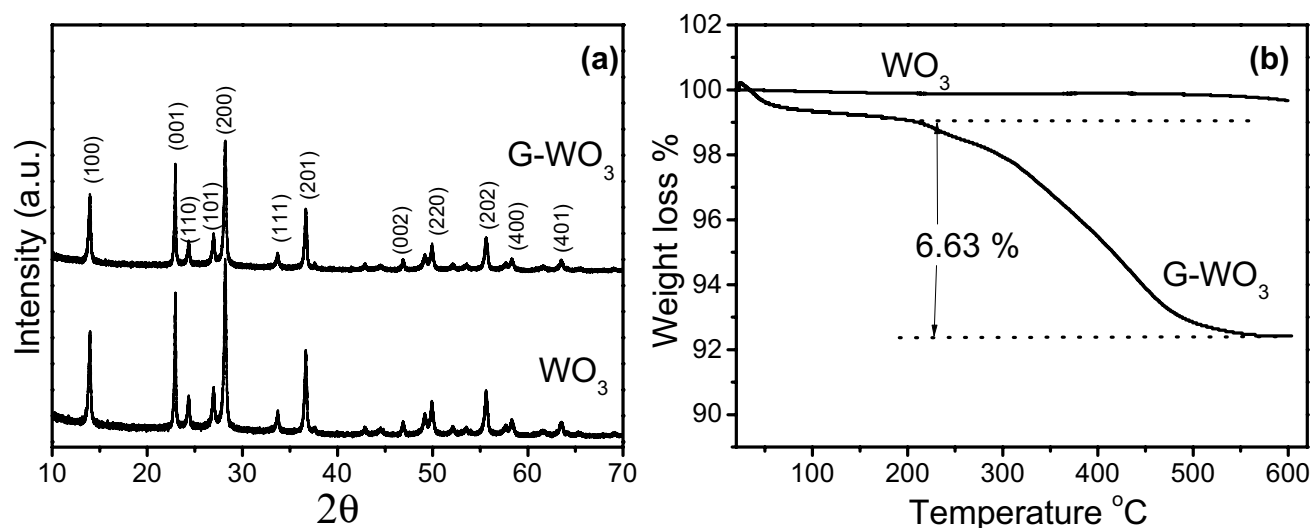**Fig. 1** **a** X-ray diffraction (XRD) patterns and **b** thermogravimetric analysis for pristine WO_3 and G–WO_3

$c = 3.8990$ Å. The average crystallite size is estimated using the Scherrer equation [35, 36]. From the full width at half maximum (FWHM) at the (100) peak ($2\theta = 13.90°$), the crystallite size is determined to be approximately 33.4 nm and 32.2 nm, respectively, for WO_3 and G–WO_3.

The TEM images (Fig. 2) clearly show that WO_3 nanoparticles are anchored to the graphene surface. The TEM image of the pristine WO_3 nanoparticles is also shown in Fig. 2c. Elemental mapping performed using scanning electron microscopy shows distribution of C, W and O in G–WO_3 (Fig. S1 in supplementary information). It is observed that there is formation of random aggregation of nanoparticles. The formation of WO_3 nanoparticles in the described method is trivial. In general, adequate acidification of an aqueous solution of Na_2WO_4 results in the formation of yellow H_2WO_4 particles. These particles when heated in air at high temperatures (> 200 °C) produced conversion of WO_3 according to the following reaction: $H_2WO_4 \rightarrow WO_3 + H_2O$. Since there is no capping agent, the formed WO_3 nanoparticles tend to randomly aggregate.

The graphene contents in all graphene–WO_3 are estimated from the yield of the synthesis. In our experiments, 10 mg, 20 mg, 30 mg, 40 mg and 50 mg of graphene correspond to its percentage weight of 1.4 wt %, 2.8 wt %, 4.25 wt %, 5.7 wt % and 7.1 wt %, respectively, in G–WO_3. TGA experiments were performed for actual quantification of the graphene content in 50 mg graphene using graphene–WO_3 composite and we found it to be 6.63% from the weight loss (Fig. 1b).The weight loss value is in close agreement with the predicted values form the yield of the synthesis. The color of the composites also changes, turning more intense gray, with increase in the concentration of graphene as shown in Fig. S2.

Figure 3 shows the UV–visible absorption spectra of all G–WO_3 composites. Excitonic feature (considering the point around which the optical absorption increases sharply in the UV–visible spectrum) of pristine WO_3 appears around 430 nm. There is lack of unanimous value for the excitonic point and, hence, the band gap energy of WO_3 in the literature
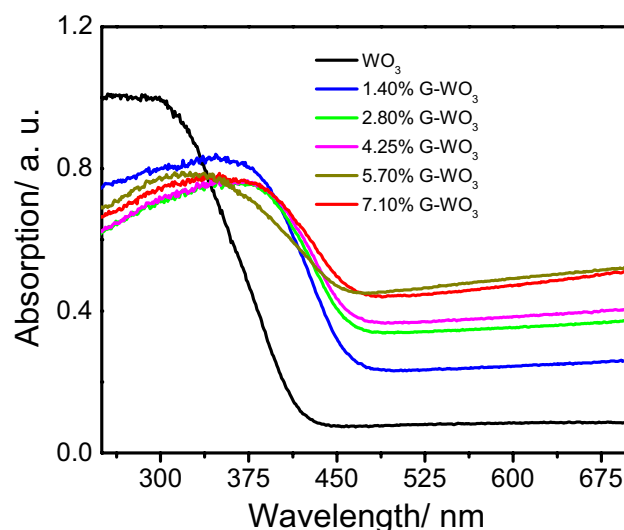

Fig. 3 UV–visible absorption spectra of G–WO_3

[37–47]. Generally, band gap energy of WO_3 $h\upsilon$is in the range of 2.6–3.0 eV, which corresponds to excitonic wavelength range of 410–500 nm [37–48]. The optical band gap energy of all the graphene–WO_3 composites was evaluated by the well-known and widely used Tauc equation [49]. According to Tauc equation, the photon energy ($h\upsilon$) is related to optical band gap energy (E_g) of a semiconductor $(\alpha h\upsilon)^{1/n}$ by the following relationship:

$$\alpha h\upsilon = A(h\upsilon - E_g)^n, \tag{1}$$

where α and A are absorption coefficient and optical transition-dependent constant of the material under investigation, $h\upsilon$ is the energy of the photon, and E_g is the band gap energy of the material. The exponent "n" indicates the nature of optical transition in the semiconductor. For allowed indirect and direct optical transitions, the values of n are respectively 2 and 0.5 [50]. Optical band gap energy can be estimated by extrapolating the linear portion near the onset on the plot of versus $h\upsilon$. Considering the nature of optical transition in
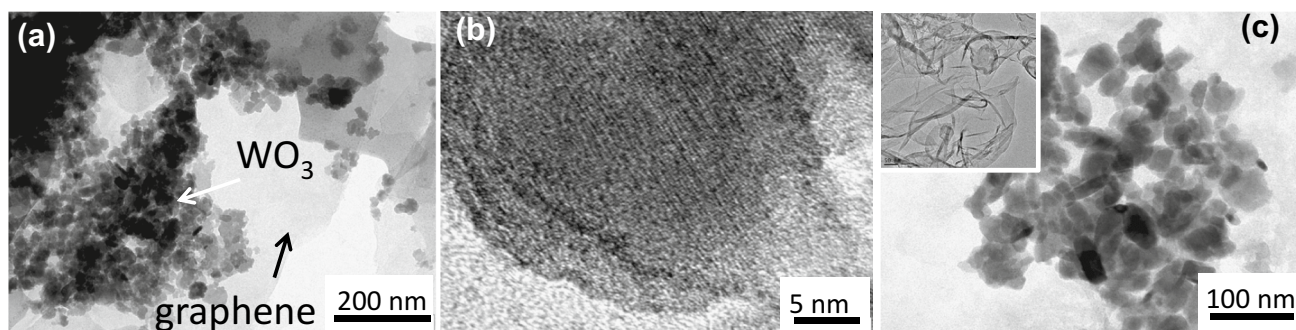

Fig. 2 TEM micrographs of **a, b** G–WO_3, **c** pristine WO_3. Inset of **c** represents the pristine graphene

WO$_3$ as indirect transition [48], the band gaps for the respective graphene–WO$_3$ composites were evaluated as shown in Fig. 4 and Fig. S3 (in supplementary information). The estimated band gap values for all the nanocomposites are summarized in Table 1. Figure 4c shows the variation of band gap of G–WO$_3$ with grapheme concentration. It is evident that band gap continuously decreases (suggesting redshift) with increasing concentration of graphene in nanocomposites. It implies that a wide band gap semiconductor could be transformed to a very narrow band gap one by anchoring the semiconductor to an optimized amount of graphene. This appears to be an interesting finding. However, ironically, the UV–visible absorption spectra of G–WO$_3$ nanocomposites were found not to be in corroboration with these above-stated dramatic band gap narrowing values (Fig. 3). It is evident that there is redshift, but a band gap value of 1.46 eV (for 7.1 wt % graphene–WO$_3$ composite) corresponds to an excitonic absorption edge near the photon wavelength of 850 nm. Surprisingly, the adsorption edge is near 480 nm for G–WO$_3$ (Fig. 3) suggesting an energy value of 2.58 eV. Therefore, the thus obtained band gap values stated above seem to be misleading. It is noteworthy that this particular method mentioned above is very often employed for determination of band gap energy of inorganic semiconductors [37–47, 51–56]. This mismatch in evaluation of energy band gap (using Tauc equation) has become an incentive for us to further access artifacts, if any, in band gap narrowing (with increase of graphene content in G–WO$_3$). For this, we have used a modified form of Tauc equation [57, 58] as outlined below.

Equation (1) can be written in a differential form as follows:

$$\frac{d\,(\ln \alpha h\upsilon)}{d\,(h\upsilon)} = \frac{n}{h\upsilon - E_g}. \tag{2}$$

The above equation suggests that there exists divergence or discontinuity in the plot of $\frac{d\,(\ln \alpha h\upsilon)}{d\,(h\upsilon)}$ versus $h\upsilon$ at $h\upsilon = E_g$.

Table 1 Estimated values of band gap energy by extrapolation and differential methods

Graphene concentration (wt %)	Band gap of G–WO$_3$	
	Extrapolation method	Differential method
0	2.67	3.01
1.40	2.24	2.89
2.80	1.85	2.83
4.25	2.02	2.83
5.70	1.63	2.81
7.10	1.46	2.81

Therefore, the divergence point in the plot of $\frac{d\,(\ln \alpha h\upsilon)}{d\,(h\upsilon)}$ versus $h\upsilon$ signifies the optical band gap energy without any assumption about the nature of the optical transitions. It is noted here that the previous method demands direct assumption of direct or indirect nature of the semiconductor, which may not be correct at times for an unknown semiconductor. The experimentally obtained optical absorption curves do not show sharp transitions at $h\upsilon = E_g$ (Fig. 3). A sloping absorption is commonly present in the optical spectra at $h\upsilon < E_g$. Therefore, the plot shows a maximum and the band gap energy is determined from the maximum [58]. The $\frac{d\,(\ln \alpha h\upsilon)}{d\,(h\upsilon)}$ versus $h\upsilon$ plots are shown in Fig. 5 and Fig. S4 (in supplementary information). The estimated band gap energies in this manner are summarized in Table 1. Figure 5c shows the variation of band gap energies of G–WO$_3$ with graphene concentrations. It is apparent that the band gap initially decreases for G–WO$_3$ with increasing concentration of graphene before reaching saturation. The saturation point (that implies maximum change) in the change of band gap is only 6.6% (inset of Fig. 5c). It is phenomenally in contrast to the results obtained using Eq. (1). Thus, the results obtained
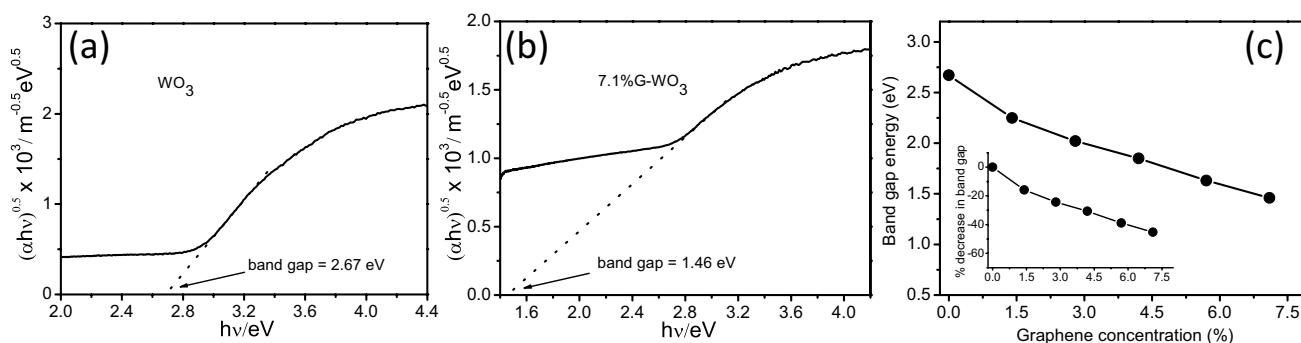

Fig. 4 Band gap energy estimation using extrapolation method for **a** pristine WO$_3$ and **b** 7.1 wt% G–WO$_3$, **c** band gap energy variation with graphene concentration obtained using extrapolation method. Inset shows percentage decrease of band gap energy with graphene concentration
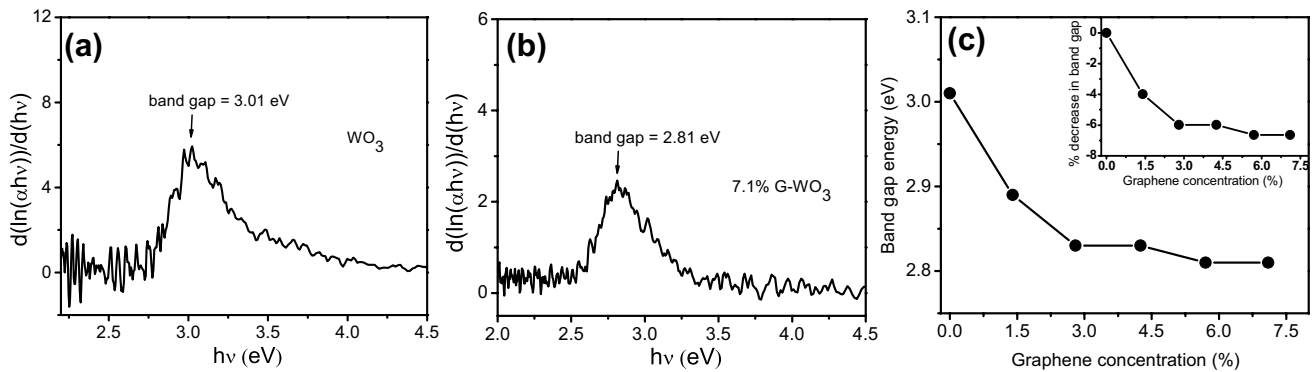
Fig. 5 Band gap energy estimation using differential method for **a** pristine WO₃ and **b** 7.1 wt% G–WO₃, **c** band gap energy variation with graphene concentration obtained using the differential method. Inset shows percentage decrease of band gap energy with graphene concentration

using Eq. (2) are more realistic and in close corroboration with the UV–visible spectra.

4 Conclusion

In summary, nanoparticles of WO₃ are anchored to graphene by simple sol–gel procedures. We observed that grapheme content in the nanocomposites plays a vital role in tuning the optical band gap of WO₃. Redshift is observed for G–WO₃ composites with increase in graphene content. Band gap narrowing of 6.6% is observed for 7.1 wt% G–WO₃ nanocomposite. We also observed saturation in the shift. We also stressed on the fact that the method of evaluation of the optical band gap is notably important. While the extrapolation method of Tauc equation is widely used for estimating the band gap energy of direct/indirect semiconductors, the present work manifests the differential method of Tauc equation for better evaluation of the band gap without reckoning the nature of optical transitions.

References

1. K.S. Novoselov, A.K. Geim, S.V. Morozov, D. Jiang, Y. Zhang, S.V. Dubonos, I.V. Grigorieva, A.A. Firsov, Science **306**, 666 (2004)
2. K.S. Novoselov, D. Jiang, F. Schedin, T.J. Booth, V.V. Khotkevich, S.V. Morozov, A.K. Geim, Proc. Natl. Acad. Sci. USA **102**, 10451 (2005)
3. F. Bonaccorso, Z. Sun, T. Hasan, A. C. Ferrari, Nature Photonics **4**, 611 (2010)
4. W. Han, R.K. Kawakami, M. Gmitra, J. Fabian, Nature Nanotech. **9**, 794 (2014)
5. N.M. Gabor, J.C.W. Song, Q. Ma, N.L. Nair, T. Taychatanapat, K. Watanabe, T. Taniguchi, L.S. Levitov, P.J. Herrero, Science **334**, 648 (2011)
6. N. Kheirabadi, A. Shafiekhani, M. Fathipour, Superlattices Microstruct. **74**, 123 (2014)
7. M. Liu, X. Yin, E.U. Avila, B. Geng, T. Zentgraf, L. Ju, F. Wang, X. Zhang, Nature **474**, 64 (2011)
8. R. Raccichini, A. Varzi, S. Passerini, B. Scrosati, Nature Mater. **14**, 271 (2015)
9. K.S. Kim, Y. Zhao, H. Jang, S.Y. Lee, J.M. Kim, K.S. Kim, J.H. Ahn, P. Kim, J.Y. Choi, B. H. Hong, Nature **457**, 706 (2009)
10. H. Park, P.R. Brown, V. Bulović, J. Kong, Nano Lett. **12**, 133 (2012)
11. Y. Shao, J. Wang, H. Wu, J. Liu, I.A. Aksay, Y. Lin, Electroanalysis **22**, 1027 (2010)
12. Y.B. Zhang, Y.W. Tan, H.L. Stormer, P. Kim, Nature **438**, 201 (2005)
13. R. Nair, P. Blake, A. Grigorenko, K. Novoselov, T. Booth, T. Stauber, N. Peres, A. Geim, Science **320**, 1308 (2008)
14. S. Balandin, W.Z. Ghosh, I. Bao, D. Calizo, F. Teweldebrhan, C.N. Miao, Lau, Nano Lett. **8**, 902 (2008)
15. K.I. Bolotin, K.J. Sikes, Z. Jiang, M. Klima, G. Fudenberg, J. Hone, P. Kim, H.L. Stormer, Solid State Commun. **146**, 351 (2008)
16. C. Lee, X. Wei, J.W. Kysar, J. Hone, Science **321**, 385 (2008)
17. S.H. Lee, M. Choi, T.–T. Kim, S. Lee, M. Liu, X. Yin, H.K. Choi, S.S. Lee, C.–G. Choi, S. Choi, X. Zhang, B. Min, Nat. Mater. **11**, 936 (2012)
18. F.J.G. Abajo, Science **339**, 917 (2013)
19. B. Gerislioglu, A. Ahmadivand, N. Pala, Opt. Mater. **73**, 729 (2017)
20. B. Ahmadivand, N. Gerislioglu, N. Pala, Phys. Status Solidi RRL **11**, 1700285 (2017)
21. X. Huang, X. Qi, F. Boey, H. Zhang, Chem. Soc. Rev. **41**, 666 (2012)
22. T. Ramanathan, A.A. Abdala, S. Stankovich, D.A. Dikin, M.H. Alonso, R.D. Piner, D.H. Adamson, H.C. Schniepp, X. Chen, R.S. Ruoff, S.T. Nguyen, I.A. Aksay, R. K. Prud'Homme, L. C. Brinson, Nature Nanotech. **3**, 327 (2008)
23. J. Wang, Z. Li, G. Fan, H. Pan, Z. Chen, D. Zhang, Scr. Mater **66**, 594 (2012)
24. D. Wang, D. Choi, J. Li, Z. Yang, Z. Nie, R. Kou, D. Hu, C. Wang, L.V. Saraf, J. Zhang, I.A. Aksay, J. Liu, ACS Nano **3**, 907 (2009)
25. S.K. Das, B. Jache, H. Lahon, C.L. Benrad, J. Janek, P. Adelhem, Chem. Commun. **52**, 1428 (2016)

26. Z. Yan, G. Liu, J. Khan, A.A. Balandin, Nature Commum. **3**, 827 (2012)
27. D.I. Son, B.W. Kwon, D.H. Park, W.S. Seo, Y. Yi, B. Angadi, C.L. Lee, K. Choi, Nature Nanotech. **7**, 465 (2012)
28. S.H. Baeck, K.S. Choi, T.F. Jaramillo, G.D. Stucky, E.W. McFarland, Adv Mater. **15**, 1269 (2003)
29. C. Santato, M. Odziemkowski, M. Ulmann, J. Augustynski, J. Am. Chem. Soc. **123**, 10639 (2001)
30. H. Zheng, J.Z. Ou, M.S. Strano, R.B. Kaner, A. Mitchell, K.K. Zadeh, Adv. Funct. Mater. **21**, 2175 (2011)
31. W.J. Li, Z.W. Fu, Appl. Surface Sc. **256**, 2447 (2010)
32. R. Asahi, T. Morikawa, T. Ohwaki, K. Aoki, Y. Taga, Science **293**, 269 (2001)
33. V. Kocevski, O. Eriksson, J. Rusz, Phys. Rev. B **87**, 245401 (2013)
34. J.T. Jensen, A.G. Ulyashin, O.M. Løvvik, J. Appl. Phys. **119**, 015702 (2016)
35. P. Scherrer, Nachr. Ges. Wiss. Göttingen **26**, 98 (1918)
36. J.I. Langford, A.J.C. Wilson, J. Appl. Cryst. **11**, 102 (1978)
37. D.G. Barton, M. Shtein, R.D. Wilson, S.L. Soled, E. Iglesia, J. Phys. Chem. B **103**, 630 (1999)
38. L. Gan, L. Xu, S. Shang, X. Zhou, L. Meng, Ceram. Int. **42**, 15235 (2016)
39. P.–Q. Wang, Y. Bai, P. -Ya Luo, J.-Y. Liu, Catal. Commun. **38**, 82 (2013)
40. R.S. Vemuri, M.H. Engelhard, C.V. Ramana, ACS Appl. Mater. Interfaces **4**, 1371 (2012)
41. X. Hu, P. Xu, H. Gong, G. Yin, Materials **11**, 147 (2018)
42. J.E. Yourey, B.M. Bartlett, J. Mater. Chem. **21**, 7651 (2011)
43. L. Fu, T. Xia, Y. Zheng, J. Yang, A. Wang, Z. Wang, Ceram. Int. **41**, 5903 (2015)
44. H. Huang, Z. Yue, G. Li, X. Wang, J. Huang, Y. Du, P. Yan, J. Mater. Chem. A **1**, 15110 (2013)
45. W. Zhu, F. Sun, R. Goei, Y. Zhou, Appl. Catal. B **207**, 93 (2017)
46. J. Cai, X. Wu, S. Li, F. Zheng, ACS Sustainable Chem. Eng. **4**, 1581 (2016)
47. Y. Liu, W. Li, J. Li, Y. Yang, Q. Chen, RSC Adv. **4**, 3219 (2014)
48. P.P. González-Borrero, F. Sato, A.N. Medina, M.L. Baesso, A.C. Bento, G. Baldissera, C. Persson, G.A. Niklasson, C.G. Granqvist, A. F. da Silva, Appl. Phys. Lett., **96**, 061909 (2010)
49. J. Tauc, R. Grigorvici, Y. Yanca, Phys. Stat. Sol. **15**, 627 (1966)
50. J.I. Pankove, *Optical Processes in Semiconductors* (Dover Publications, New York, 1971)
51. J.S. Lee, K.H. You, C.B. Park, Adv. Mater. **24**, 1084 (2012)
52. Y. Zhang, Z.R. Tang, X. Fu, Y.J. Xu, ACS Nano **4**, 7303 (2010)
53. W. Fan, Q. Lai, Q. Zhang, Y. Wang, J. Phys. Chem. C **115**, 10694 (2011)
54. S. Joishy, B.V. Rajendra, Appl. Phys. A **123**, 711 (2017)
55. Y. Li, Y. Tang, F. Wang, X. Zhao, J. Chen, Z. Zeng, L. Yang, H. Luo, Appl. Phys. A **124**, 276 (2018)
56. B.J. Rani, M. Durga, G. Ravi, P. Krishnaveni, V. Ganesh, S. Ravichandran, R. Yuvakkumar, Appl. Phys. A **124**, 319 (2018)
57. S.K. Panda, S. Chakrabarti, B. Satpati, P.V. Satyam, S. Chaudhuri, J. Phys. D: Appl. Phys. **37**, 628 (2004)
58. M.B. Johansson, G. Baldissera, I. Valyukh, C. Persson, H. Arwin, G.A. Niklasson, L. Osterlund, J. Phys.: Condens. Matter. **25**, 205502 (2013)